

Simulating train-tunnel aerodynamics with a parallel adaptive Cartesian method

Ralf Deiterding and Jose M. Garro Fernandez

Aerodynamics and Flight Mechanics Research Group
University of Southampton
Highfield Campus, Southampton SO17 1BJ, UK
E-mail: r.deiterding@soton.ac.uk

June 5, 2019

Outline

Adaptive Cartesian finite volume methods

- Block-structured AMR with complex boundaries
- Parallelization approach

Train-tunnel aerodynamics

- Validation
- Passing trains in open space
- Passing trains in a double track tunnel

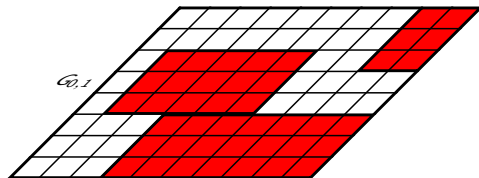
Conclusions

- Summary and outlook

Block-structured adaptive mesh refinement (SAMR)

For simplicity $\partial_t \mathbf{q}(x, y, t) + \partial_x \mathbf{f}(\mathbf{q}(x, y, t)) + \partial_y \mathbf{g}(\mathbf{q}(x, y, t)) = 0$

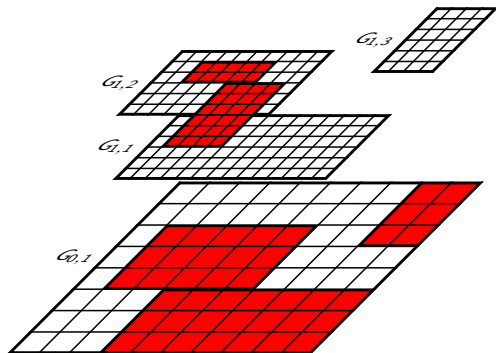
- Refined blocks overlay coarser ones



Block-structured adaptive mesh refinement (SAMR)

For simplicity $\partial_t \mathbf{q}(x, y, t) + \partial_x \mathbf{f}(\mathbf{q}(x, y, t)) + \partial_y \mathbf{g}(\mathbf{q}(x, y, t)) = 0$

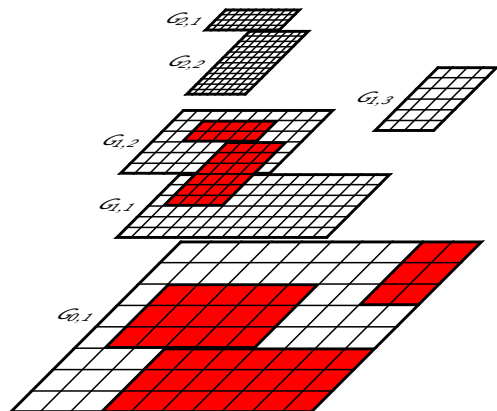
- Refined blocks overlay coarser ones



Block-structured adaptive mesh refinement (SAMR)

For simplicity $\partial_t \mathbf{q}(x, y, t) + \partial_x \mathbf{f}(\mathbf{q}(x, y, t)) + \partial_y \mathbf{g}(\mathbf{q}(x, y, t)) = 0$

- Refined blocks overlay coarser ones



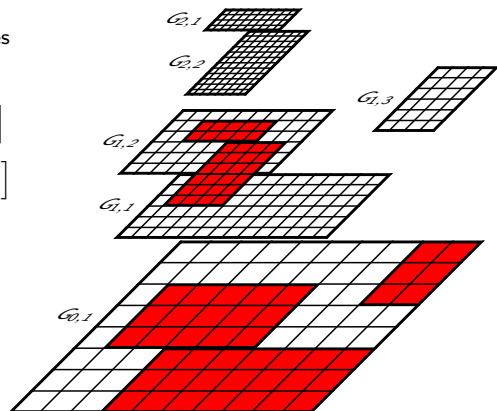
Block-structured adaptive mesh refinement (SAMR)

For simplicity $\partial_t \mathbf{q}(x, y, t) + \partial_x \mathbf{f}(\mathbf{q}(x, y, t)) + \partial_y \mathbf{g}(\mathbf{q}(x, y, t)) = 0$

- ▶ Refined blocks overlay coarser ones
- ▶ Refinement in space *and* time by factor r_l
[Berger and Colella, 1988]
- ▶ Block (aka patch) based data structures
- + Numerical scheme

$$\mathbf{Q}_{jk}^{n+1} = \mathbf{Q}_{jk}^n - \frac{\Delta t}{\Delta x} \left[\mathbf{F}_{j+\frac{1}{2},k} - \mathbf{F}_{j-\frac{1}{2},k} \right] - \frac{\Delta t}{\Delta y} \left[\mathbf{G}_{j,k+\frac{1}{2}} - \mathbf{G}_{j,k-\frac{1}{2}} \right]$$

only for single patch necessary



Block-structured adaptive mesh refinement (SAMR)

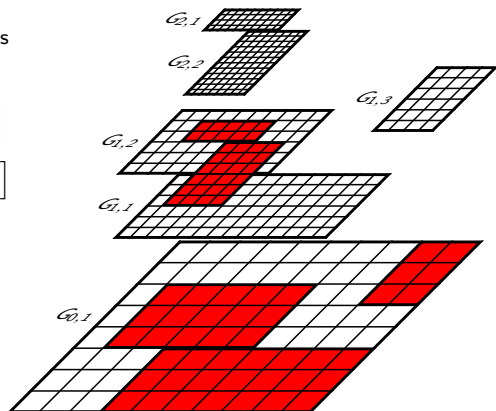
For simplicity $\partial_t \mathbf{q}(x, y, t) + \partial_x \mathbf{f}(\mathbf{q}(x, y, t)) + \partial_y \mathbf{g}(\mathbf{q}(x, y, t)) = 0$

- ▶ Refined blocks overlay coarser ones
- ▶ Refinement in space *and* time by factor r_l
[Berger and Colella, 1988]
- ▶ Block (aka patch) based data structures
- + Numerical scheme

$$\mathbf{Q}_{jk}^{n+1} = \mathbf{Q}_{jk}^n - \frac{\Delta t}{\Delta x} \left[\mathbf{F}_{j+\frac{1}{2},k} - \mathbf{F}_{j-\frac{1}{2},k} \right] - \frac{\Delta t}{\Delta y} \left[\mathbf{G}_{j,k+\frac{1}{2}} - \mathbf{G}_{j,k-\frac{1}{2}} \right]$$

only for single patch necessary

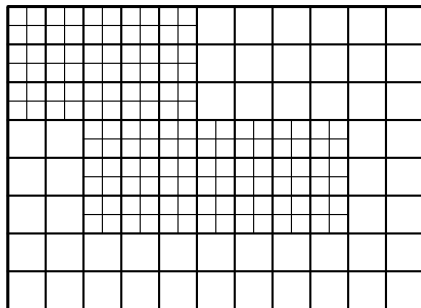
- + Efficient cache-reuse / vectorization possible
- Cluster-algorithm necessary
- ▶ Papers: [Deiterding, 2011a, Deiterding et al., 2009b, Deiterding et al., 2007]



Level transfer / setting of ghost cells

Conservative averaging
(restriction):

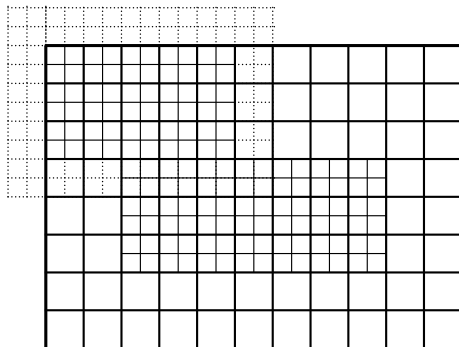
$$\hat{\mathbf{Q}}_{jk}^l := \frac{1}{(r_{l+1})^2} \sum_{\kappa=0}^{r_{l+1}-1} \sum_{\iota=0}^{r_{l+1}-1} \mathbf{Q}_{v+\kappa, w+\iota}^{l+1}$$



Level transfer / setting of ghost cells

Conservative averaging
(restriction):

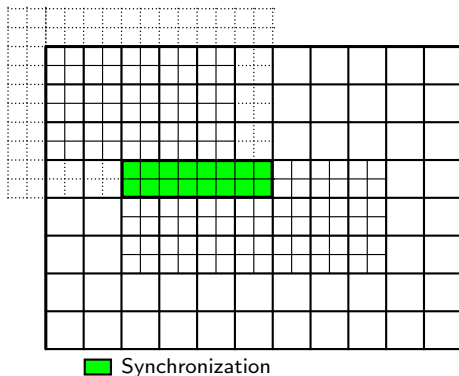
$$\hat{\mathbf{Q}}_{jk}^l := \frac{1}{(r_{l+1})^2} \sum_{\kappa=0}^{r_{l+1}-1} \sum_{\iota=0}^{r_{l+1}-1} \mathbf{Q}_{v+\kappa, w+\iota}^{l+1}$$



Level transfer / setting of ghost cells

Conservative averaging
(restriction):

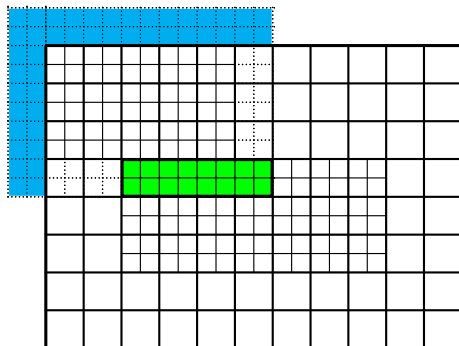
$$\hat{\mathbf{Q}}_{jk}^l := \frac{1}{(r_{l+1})^2} \sum_{\kappa=0}^{r_{l+1}-1} \sum_{\iota=0}^{r_{l+1}-1} \mathbf{Q}_{v+\kappa, w+\iota}^{l+1}$$



Level transfer / setting of ghost cells

Conservative averaging
(restriction):

$$\hat{\mathbf{Q}}_{jk}^l := \frac{1}{(r_{l+1})^2} \sum_{\kappa=0}^{r_{l+1}-1} \sum_{\iota=0}^{r_{l+1}-1} \mathbf{Q}_{v+\kappa, w+\iota}^{l+1}$$



Synchronization

Physical boundary conditions

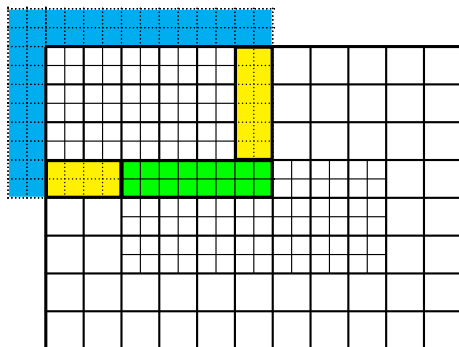
Level transfer / setting of ghost cells

Conservative averaging
(restriction):

$$\hat{\mathbf{Q}}'_{jk} := \frac{1}{(r_{l+1})^2} \sum_{\kappa=0}^{r_{l+1}-1} \sum_{\iota=0}^{r_{l+1}-1} \mathbf{Q}_{v+\kappa, w+\iota}^{l+1}$$

Bilinear interpolation
(prolongation):

$$\begin{aligned} \check{\mathbf{Q}}_{vw}^{l+1} := & (1 - f_1)(1 - f_2) \mathbf{Q}'_{j-1, k-1} \\ & + f_1(1 - f_2) \mathbf{Q}'_{j, k-1} + \\ & (1 - f_1)f_2 \mathbf{Q}'_{j-1, k} + f_1 f_2 \mathbf{Q}'_{jk} \end{aligned}$$



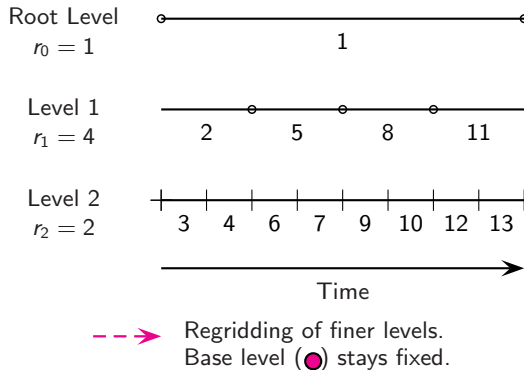
- Synchronization
- Physical boundary conditions
- Interpolation

For boundary conditions: linear time interpolation

$$\tilde{\mathbf{Q}}^{l+1}(t + \kappa \Delta t_{l+1}) := \left(1 - \frac{\kappa}{r_{l+1}}\right) \check{\mathbf{Q}}^{l+1}(t) + \frac{\kappa}{r_{l+1}} \check{\mathbf{Q}}^{l+1}(t + \Delta t_l) \quad \text{for } \kappa = 0, \dots, r_{l+1}$$

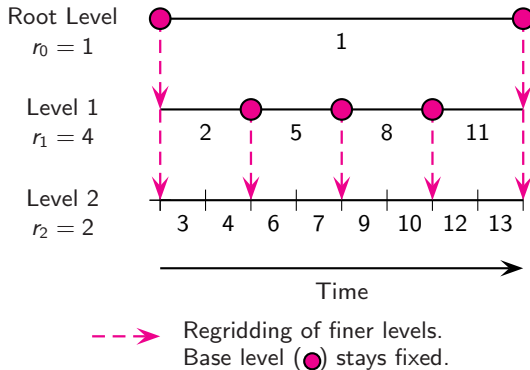
Recursive integration order

- Space-time interpolation of coarse data to set $l_l^s, l > 0$

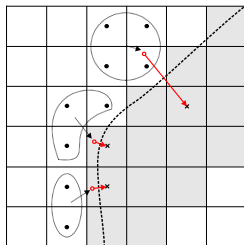


Recursive integration order

- ▶ Space-time interpolation of coarse data to set $I_l^s, l > 0$
- ▶ Regriding:
 - ▶ Creation of new grids, copy existing cells on level $l > 0$
 - ▶ Spatial interpolation to initialize new cells on level $l > 0$

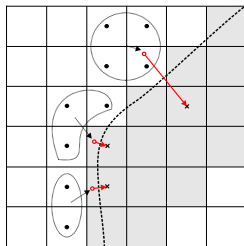


Level-set method for boundary embedding



- ▶ Implicit boundary representation via distance function φ , normal $\mathbf{n} = \nabla\varphi/|\nabla\varphi|$
- ▶ Complex boundary moving with local velocity \mathbf{w} , treat interface as moving rigid wall [Deiterding et al., 2007]
- ▶ Construction of values in embedded boundary cells by interpolation / extrapolation [Deiterding, 2009, Deiterding, 2011a]
- ▶ Creation of level set from triangulated surface data with closest-point-transform (CPT) algorithm [Mauch, 2003, Deiterding et al., 2006]

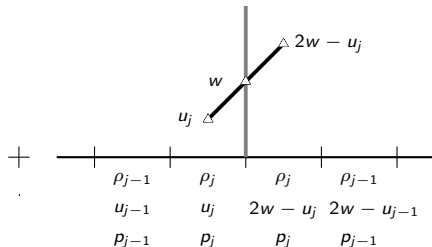
Level-set method for boundary embedding



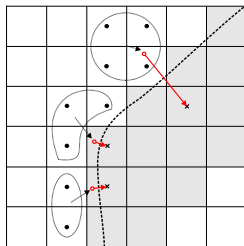
Interpolate / constant value extrapolate values at

$$\tilde{\mathbf{x}} = \mathbf{x} + 2\varphi \mathbf{n}$$

- ▶ Implicit boundary representation via distance function φ , normal $\mathbf{n} = \nabla \varphi / |\nabla \varphi|$
- ▶ Complex boundary moving with local velocity \mathbf{w} , treat interface as moving rigid wall [Deiterding et al., 2007]
- ▶ Construction of values in embedded boundary cells by interpolation / extrapolation [Deiterding, 2009, Deiterding, 2011a]
- ▶ Creation of level set from triangulated surface data with closest-point-transform (CPT) algorithm [Mauch, 2003, Deiterding et al., 2006]



Level-set method for boundary embedding



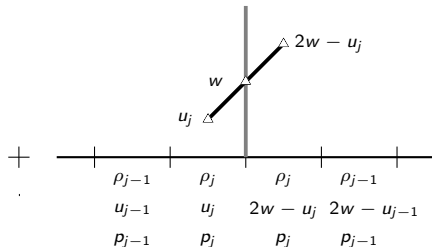
Interpolate / constant value extrapolate values at

$$\tilde{\mathbf{x}} = \mathbf{x} + 2\varphi\mathbf{n}$$

Velocity in ghost cells (slip):

$$\begin{aligned}\mathbf{u}' &= (2\mathbf{w} \cdot \mathbf{n} - \mathbf{u} \cdot \mathbf{n})\mathbf{n} + (\mathbf{u} \cdot \mathbf{t})\mathbf{t} \\ &= 2((\mathbf{w} - \mathbf{u}) \cdot \mathbf{n})\mathbf{n} + \mathbf{u}\end{aligned}$$

- ▶ Implicit boundary representation via distance function φ , normal $\mathbf{n} = \nabla\varphi/|\nabla\varphi|$
- ▶ Complex boundary moving with local velocity \mathbf{w} , treat interface as moving rigid wall [Deiterding et al., 2007]
- ▶ Construction of values in embedded boundary cells by interpolation / extrapolation [Deiterding, 2009, Deiterding, 2011a]
- ▶ Creation of level set from triangulated surface data with closest-point-transform (CPT) algorithm [Mauch, 2003, Deiterding et al., 2006]



Parallelization

Rigorous domain decomposition

- ▶ Data of all levels resides on same node
- ▶ Grid hierarchy defines unique "floor-plan"
- ▶ Workload estimation

$$\mathcal{W}(\Omega) = \sum_{l=0}^{l_{\max}} \left[\mathcal{N}_l(G_l \cap \Omega) \prod_{\kappa=0}^l r_{\kappa} \right]$$

Parallelization

Rigorous domain decomposition

- ▶ Data of all levels resides on same node
- ▶ Grid hierarchy defines unique "floor-plan"
- ▶ Workload estimation

$$\mathcal{W}(\Omega) = \sum_{l=0}^{l_{\max}} \left[\mathcal{N}_l(G_l \cap \Omega) \prod_{\kappa=0}^l r_{\kappa} \right]$$

- ▶ Parallel operations
 - ▶ Synchronization of ghost cells
 - ▶ Redistribution of data blocks within regridding operation
 - ▶ Flux correction of coarse grid cells
- ▶ Dynamic partitioning with space-filling curve

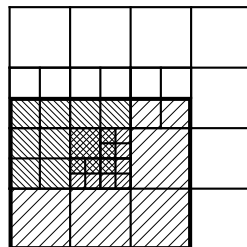
Parallelization

Rigorous domain decomposition

- ▶ Data of all levels resides on same node
- ▶ Grid hierarchy defines unique "floor-plan"
- ▶ Workload estimation

$$\mathcal{W}(\Omega) = \sum_{l=0}^{l_{\max}} \left[\mathcal{N}_l(G_l \cap \Omega) \prod_{\kappa=0}^l r_{\kappa} \right]$$

- ▶ Parallel operations
 - ▶ Synchronization of ghost cells
 - ▶ Redistribution of data blocks within regridding operation
 - ▶ Flux correction of coarse grid cells
- ▶ Dynamic partitioning with space-filling curve



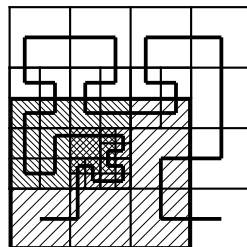
Parallelization

Rigorous domain decomposition

- ▶ Data of all levels resides on same node
- ▶ Grid hierarchy defines unique "floor-plan"
- ▶ Workload estimation

$$\mathcal{W}(\Omega) = \sum_{l=0}^{l_{\max}} \left[\mathcal{N}_l(G_l \cap \Omega) \prod_{\kappa=0}^l r_{\kappa} \right]$$

- ▶ Parallel operations
 - ▶ Synchronization of ghost cells
 - ▶ Redistribution of data blocks within regridding operation
 - ▶ Flux correction of coarse grid cells
- ▶ Dynamic partitioning with space-filling curve



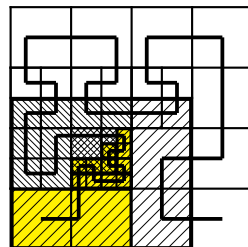
Parallelization

Rigorous domain decomposition

- ▶ Data of all levels resides on same node
- ▶ Grid hierarchy defines unique "floor-plan"
- ▶ Workload estimation

$$\mathcal{W}(\Omega) = \sum_{l=0}^{l_{\max}} \left[\mathcal{N}_l(G_l \cap \Omega) \prod_{\kappa=0}^l r_{\kappa} \right]$$

- ▶ Parallel operations
 - ▶ Synchronization of ghost cells
 - ▶ Redistribution of data blocks within regridding operation
 - ▶ Flux correction of coarse grid cells
- ▶ Dynamic partitioning with space-filling curve



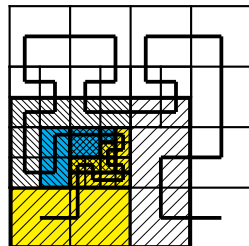
Parallelization

Rigorous domain decomposition

- ▶ Data of all levels resides on same node
- ▶ Grid hierarchy defines unique "floor-plan"
- ▶ Workload estimation

$$\mathcal{W}(\Omega) = \sum_{l=0}^{l_{\max}} \left[\mathcal{N}_l(\mathbf{G}_l \cap \Omega) \prod_{\kappa=0}^l r_{\kappa} \right]$$

- ▶ Parallel operations
 - ▶ Synchronization of ghost cells
 - ▶ Redistribution of data blocks within regridding operation
 - ▶ Flux correction of coarse grid cells
- ▶ Dynamic partitioning with space-filling curve



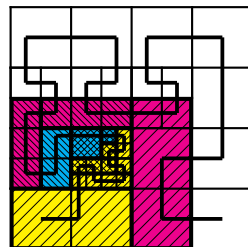
Parallelization

Rigorous domain decomposition

- ▶ Data of all levels resides on same node
- ▶ Grid hierarchy defines unique "floor-plan"
- ▶ Workload estimation

$$\mathcal{W}(\Omega) = \sum_{l=0}^{l_{\max}} \left[\mathcal{N}_l(G_l \cap \Omega) \prod_{\kappa=0}^l r_{\kappa} \right]$$

- ▶ Parallel operations
 - ▶ Synchronization of ghost cells
 - ▶ Redistribution of data blocks within regridding operation
 - ▶ Flux correction of coarse grid cells
- ▶ Dynamic partitioning with space-filling curve



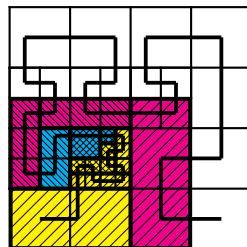
Parallelization

Rigorous domain decomposition

- ▶ Data of all levels resides on same node
- ▶ Grid hierarchy defines unique "floor-plan"
- ▶ Workload estimation

$$\mathcal{W}(\Omega) = \sum_{l=0}^{l_{\max}} \left[\mathcal{N}_l(G_l \cap \Omega) \prod_{\kappa=0}^l r_{\kappa} \right]$$

- ▶ Parallel operations
 - ▶ Synchronization of ghost cells
 - ▶ Redistribution of data blocks within regridding operation
 - ▶ Flux correction of coarse grid cells
- ▶ Dynamic partitioning with space-filling curve



[Deiterding, 2005, Deiterding, 2011a]

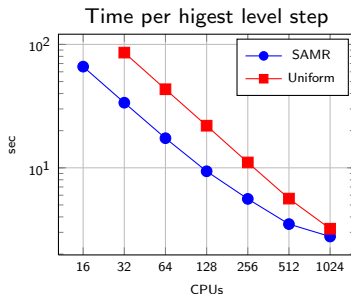
AMROC framework and most important patch solvers

- ▶ Implements described algorithms and facilitates easy exchange of the block-based numerical scheme
- ▶ Shock-induced combustion with detailed chemistry: [Deiterding, 2003, Deiterding and Bader, 2005, Deiterding, 2011b, Cai et al., 2016, Cai et al., 2018]
- ▶ Hybrid WENO methods for LES and DNS: [Pantano et al., 2007, Lombardini and Deiterding, 2010, Ziegler et al., 2011, Cerminara et al., 2018]
- ▶ Lattice Boltzmann method for LES: [Fragner and Deiterding, 2016, Feldhusen et al., 2016, Deiterding and Wood, 2016]
- ▶ FSI deformation from water hammer: [Cirak et al., 2007, Deiterding et al., 2009a, Perotti et al., 2013, Wan et al., 2017]
- ▶ Level-set method for Eulerian solid mechanics: [Barton et al., 2013]
- ▶ Ideal magneto-hydrodynamics: [Gomes et al., 2015, Souza Lopes et al., 2018]
- ▶ ~ 500,000 LOC in C++, C, Fortran-77, Fortran-90
- ▶ V2.0 plus FSI coupling routines as open source at <http://www.vtf.website>
- ▶ Used here V3.0 with significantly enhanced parallelization (V2.1 not released)

AMROC strong scalability tests

3D wave propagation method with Roe scheme:
spherical blast wave

► Tests run IBM BG/P (mode VN)



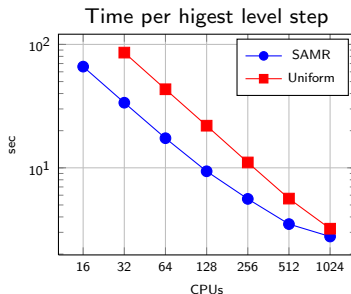
$64 \times 32 \times 32$ base grid, 2 additional levels with
factors 2, 4; uniform $512 \times 256 \times 256 = 33.6 \cdot 10^6$
cells

Level	Grids	Cells
0	1709	65,536
1	1735	271,048
2	2210	7,190,208

AMROC strong scalability tests

3D wave propagation method with Roe scheme:
spherical blast wave

► Tests run IBM BG/P (mode VN)

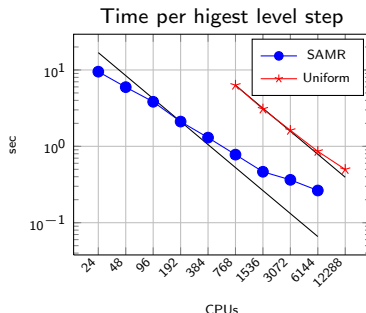


$64 \times 32 \times 32$ base grid, 2 additional levels with factors 2, 4; uniform $512 \times 256 \times 256 = 33.6 \cdot 10^6$ cells

Level	Grids	Cells
0	1709	65,536
1	1735	271,048
2	2210	7,190,208

3D SRT-lattice Boltzmann scheme: flow over rough surface of $19 \times 13 \times 2$ spheres

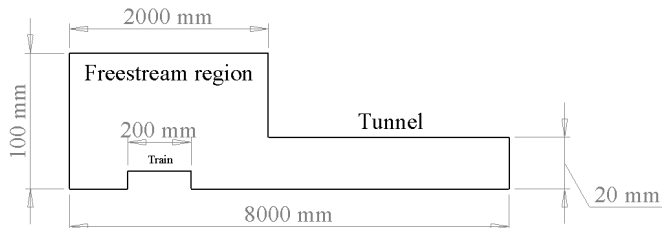
► Tests run Cray XC30m (Archer)



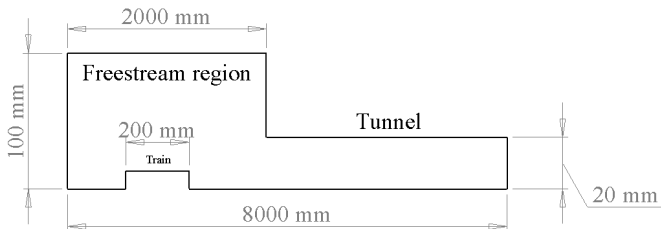
$360 \times 240 \times 108$ base grid, 2 additional levels with factors 2, 4; uniform $1440 \times 1920 \times 432 = 1.19 \cdot 10^9$ cells

Level	Grids	Cells
0	788	9,331,200
1	21367	24,844,504
2	1728	10,838,016

Laboratory tunnel simulator [Zonglin et al., 2002]



Laboratory tunnel simulator [Zonglin et al., 2002]

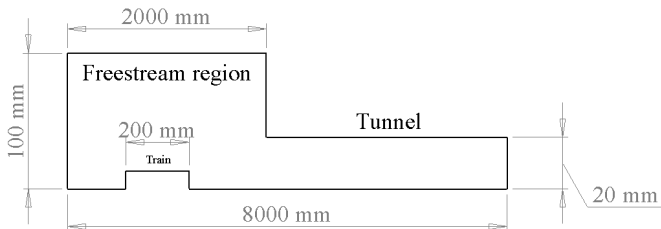


Model solves the inviscid Euler equations

$$\begin{aligned}\partial_t \rho + \nabla \cdot (\rho \mathbf{u}) &= 0 \\ \partial_t (\rho \mathbf{u}) + \nabla \cdot (\rho \mathbf{u} \otimes \mathbf{u}) + \nabla p &= 0 \\ \partial_t (\rho E) + \nabla \cdot ((\rho E + p) \mathbf{u}) &= 0\end{aligned}$$

with $p = (\gamma - 1)(\rho E - \frac{1}{2} \rho \mathbf{u}^T \mathbf{u})$

Laboratory tunnel simulator [Zonglin et al., 2002]



Model solves the inviscid Euler equations

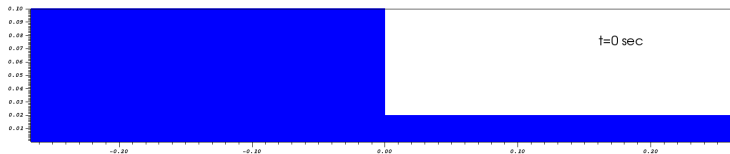
$$\begin{aligned}\partial_t \rho + \nabla \cdot (\rho \mathbf{u}) &= 0 \\ \partial_t (\rho \mathbf{u}) + \nabla \cdot (\rho \mathbf{u} \otimes \mathbf{u}) + \nabla p &= 0 \\ \partial_t (\rho E) + \nabla \cdot ((\rho E + p) \mathbf{u}) &= 0\end{aligned}$$

with $p = (\gamma - 1)(\rho E - \frac{1}{2} \rho \mathbf{u}^T \mathbf{u})$

- ▶ Two-dimensional axi-symmetric computation
- ▶ $p_0 = 100$ kPa, $\rho_0 = 1.225$ kg/m³, $\gamma = 1.4$
- ▶ Roe shock-capturing scheme blended with HLL
- ▶ 2nd order accuracy achieved with MUSCL-Hancock method

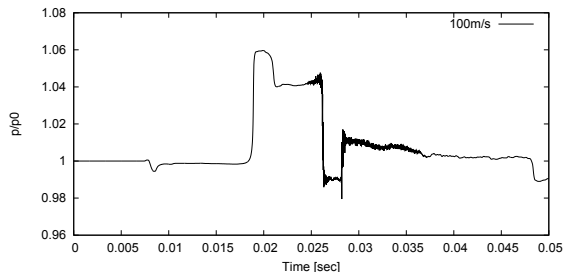
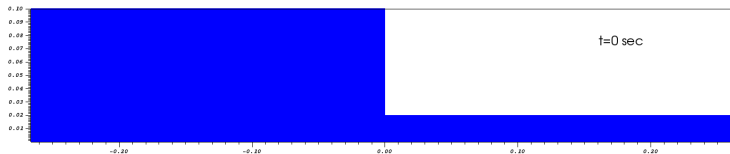
Basic phenomena – $v_0 = 100$ m/s

- ▶ 800×25 mesh with Cartesian cut-out (200, 5) to (800, 25)
- ▶ 2 level of additional refinement by factor 2



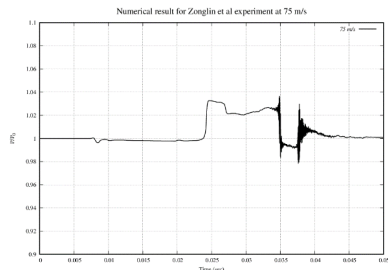
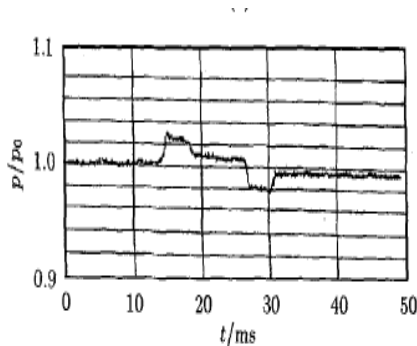
Basic phenomena – $v_0 = 100$ m/s

- ▶ 800×25 mesh with Cartesian cut-out (200, 5) to (800, 25)
- ▶ 2 level of additional refinement by factor 2



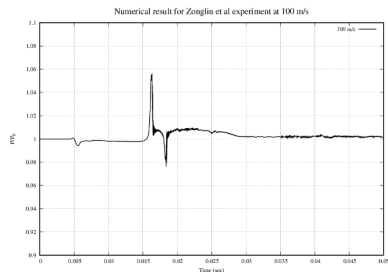
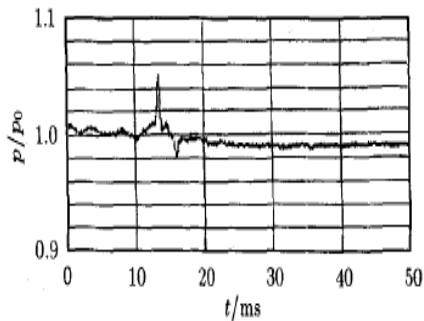
Pressure record at location (1020 mm, 20 mm) inside tunnel

Comparison with experiment – I



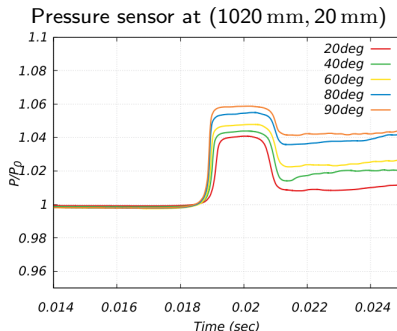
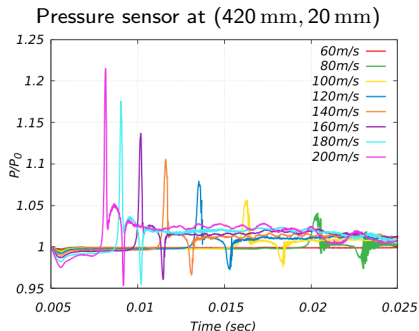
Pressure record at (1020 mm, 20 mm) for $v_0 = 75$ m/s. Experiment (left) and AMROC (right)

Comparison with experiment – I



Pressure record at (40 mm, 20 mm) for model velocity $v_0 = 100$ m/s. Experiment (left) and AMROC (right)

Variation of velocity and nose half angle



- ▶ Dependence on v_0^2 is the dynamic pressure influence (left)
- ▶ For constant blockage ratio and body velocity, using more pointed noses alleviates the maximal pressure level (right, nose half angle varied)
- ▶ For $v_0 \approx 140$ m/s a shock wave (tunnel boom) can be observed. Sharper noses also delay this phenomenon.

NGT2 prototype setup

- ▶ Next Generation Train 2 (NGT2) geometry by the German Aerospace Centre (DLR) [Fragner and Deiterding, 2016, Fragner and Deiterding, 2017]
- ▶ Mirrored train head of length ~ 60 m, no wheels or tracks, train models 0.17 m above ground above the ground level.
- ▶ Train velocities 100 m/s and -100 m/s, middle axis 6 m apart, initial distance between centers 200 m
- ▶ Base mesh of $360 \times 40 \times 30$ for domain of $360 \text{ m} \times 40 \text{ m} \times 30 \text{ m}$
- ▶ Two/three additional levels, refined by $r_{1,2,3} = 2$. Refinement based on pressure gradient and level set and regenerated at every coarse time step. Parallel redistribution at every level-0 time step.
- ▶ On 96 cores Intel Xeon E5-2670 2.6 GHz a final $t_e = 3 \text{ sec}$ was reached after 12,385 sec / 43,395 sec wall time, i.e., 330 h and 1157 h CPU

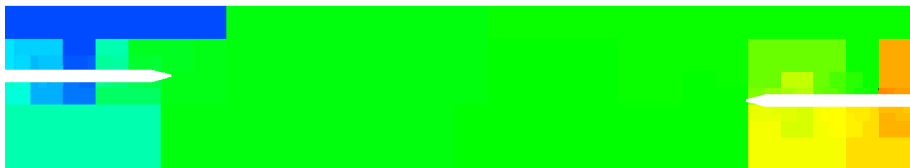


Passing in open space – AMR and dynamic distribution

Domains of three-level refinement



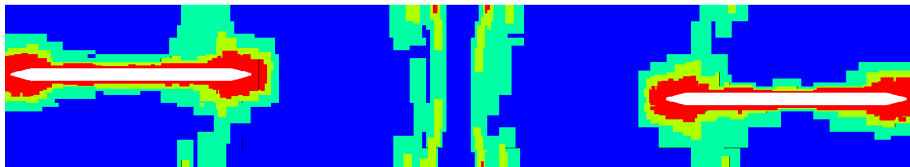
Distribution to 96 processors



Enlargement of domain center shown

Passing in open space – AMR and dynamic distribution

Domains of three-level refinement



Distribution to 96 processors



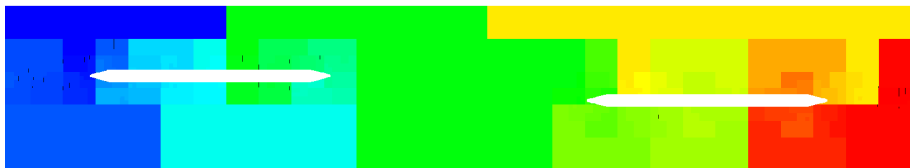
Enlargement of domain center shown

Passing in open space – AMR and dynamic distribution

Domains of three-level refinement



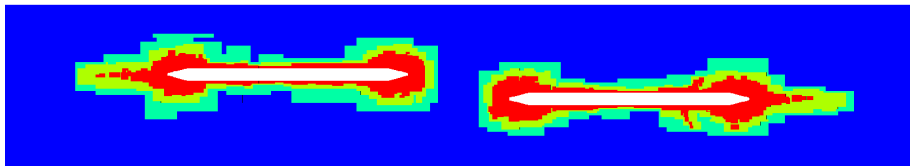
Distribution to 96 processors



Enlargement of domain center shown

Passing in open space – AMR and dynamic distribution

Domains of three-level refinement



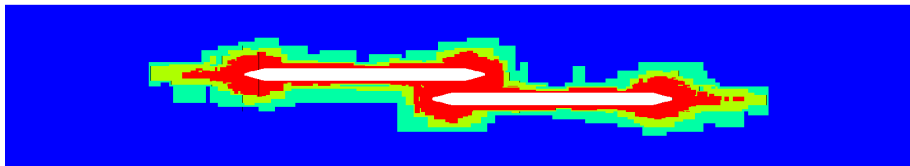
Distribution to 96 processors



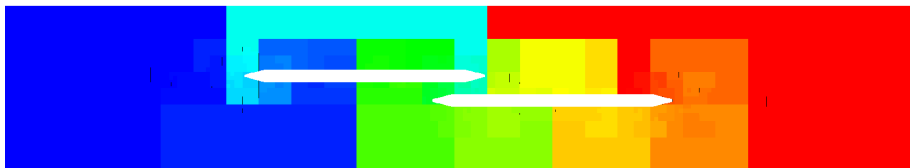
Enlargement of domain center shown

Passing in open space – AMR and dynamic distribution

Domains of three-level refinement



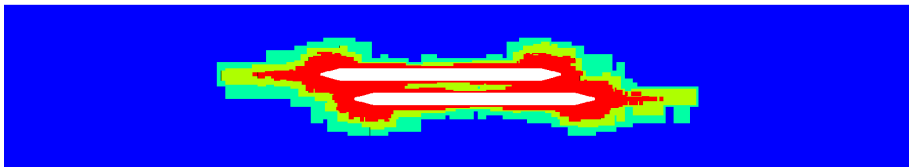
Distribution to 96 processors



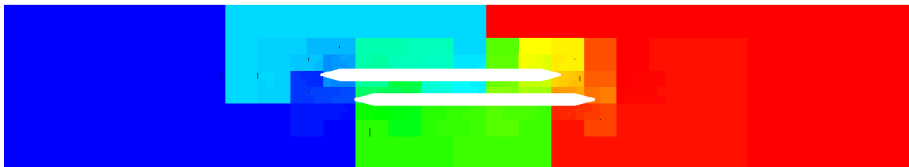
Enlargement of domain center shown

Passing in open space – AMR and dynamic distribution

Domains of three-level refinement



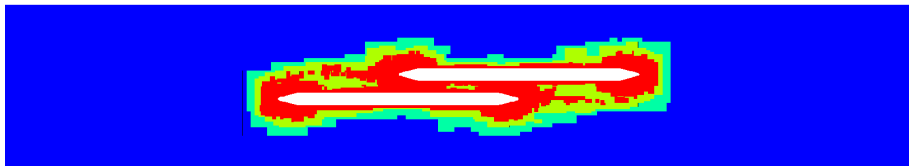
Distribution to 96 processors



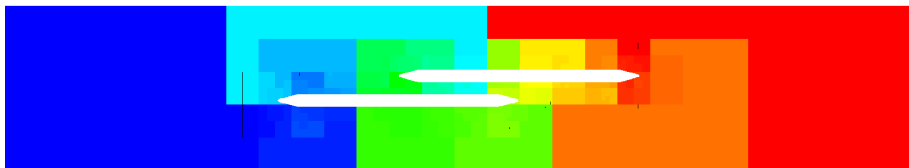
Enlargement of domain center shown

Passing in open space – AMR and dynamic distribution

Domains of three-level refinement



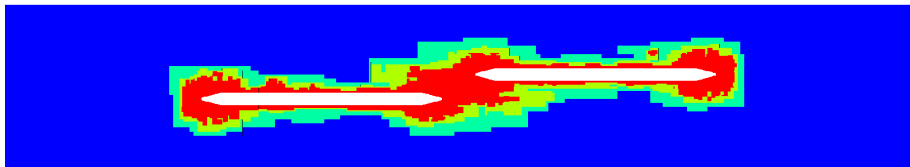
Distribution to 96 processors



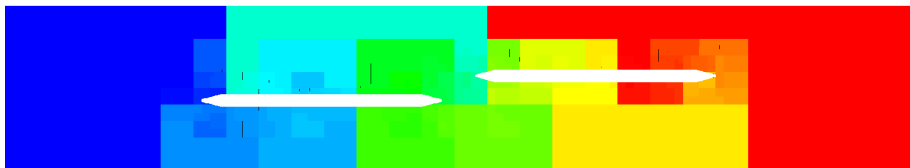
Enlargement of domain center shown

Passing in open space – AMR and dynamic distribution

Domains of three-level refinement



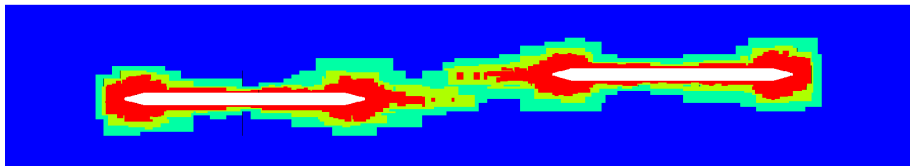
Distribution to 96 processors



Enlargement of domain center shown

Passing in open space – AMR and dynamic distribution

Domains of three-level refinement

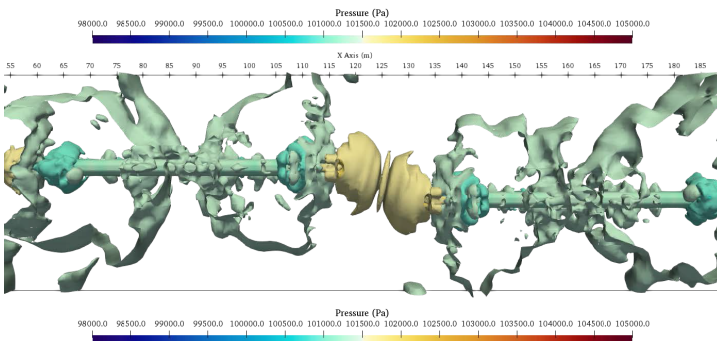
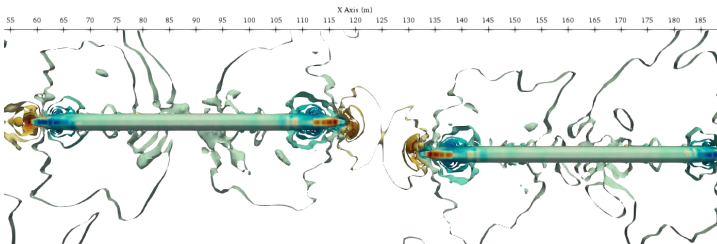


Distribution to 96 processors

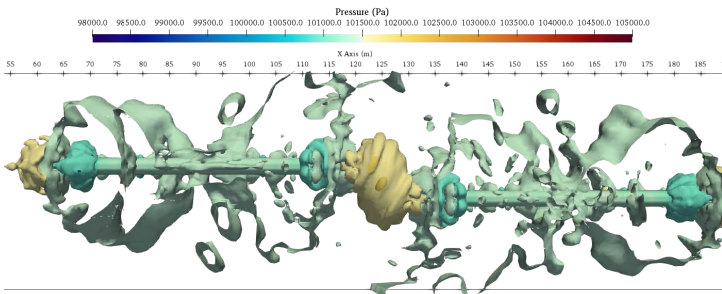
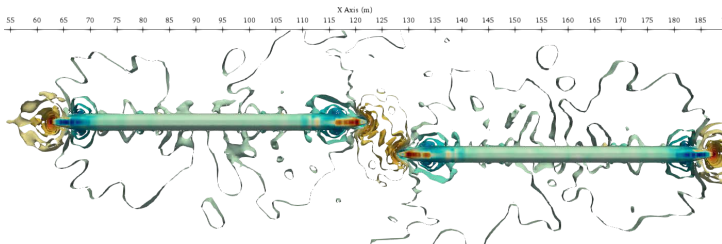


Enlargement of domain center shown

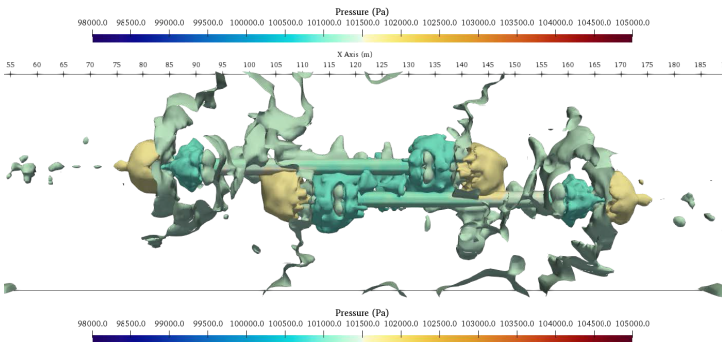
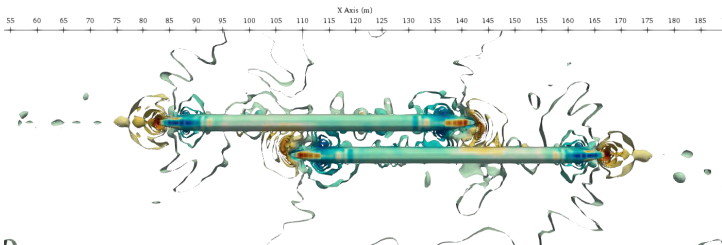
Pressure isosurfaces



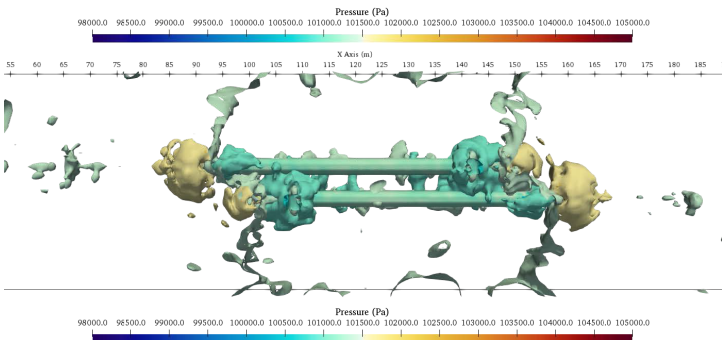
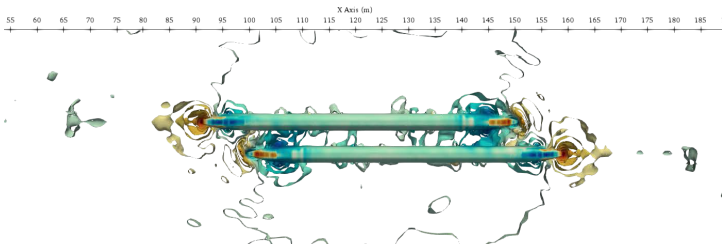
Pressure isosurfaces



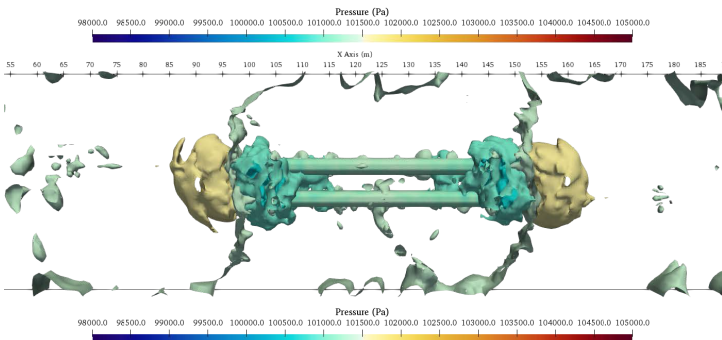
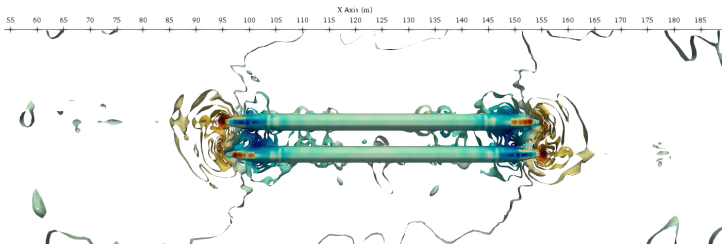
Pressure isosurfaces



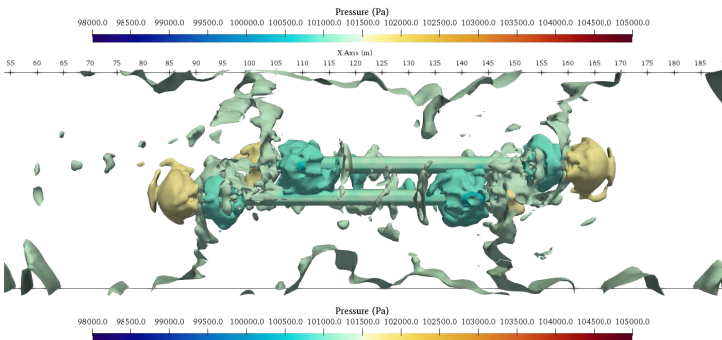
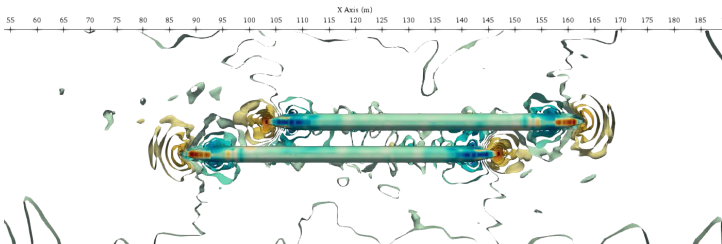
Pressure isosurfaces



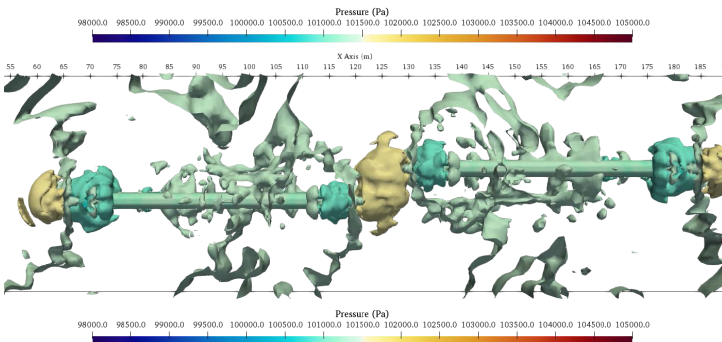
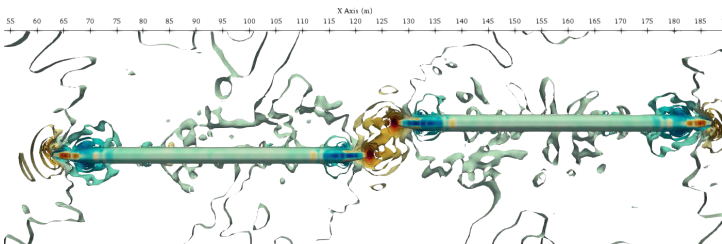
Pressure isosurfaces



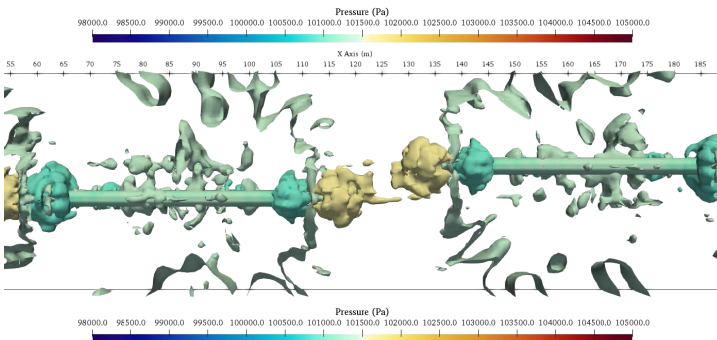
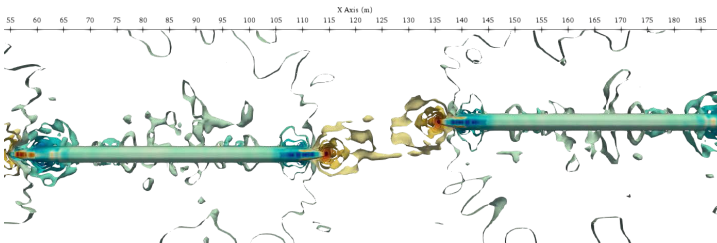
Pressure isosurfaces



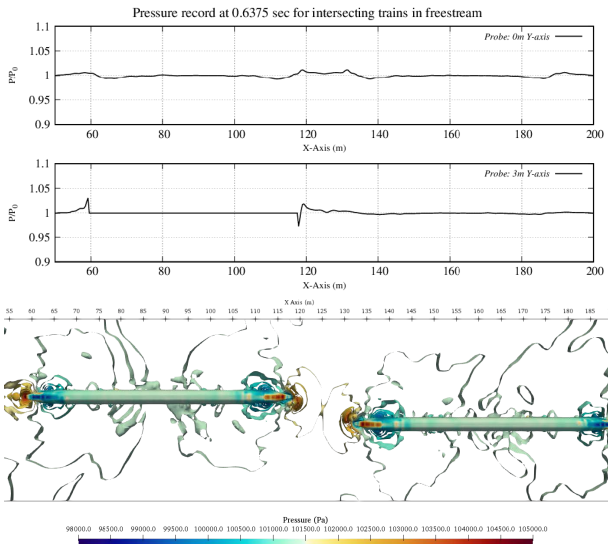
Pressure isosurfaces



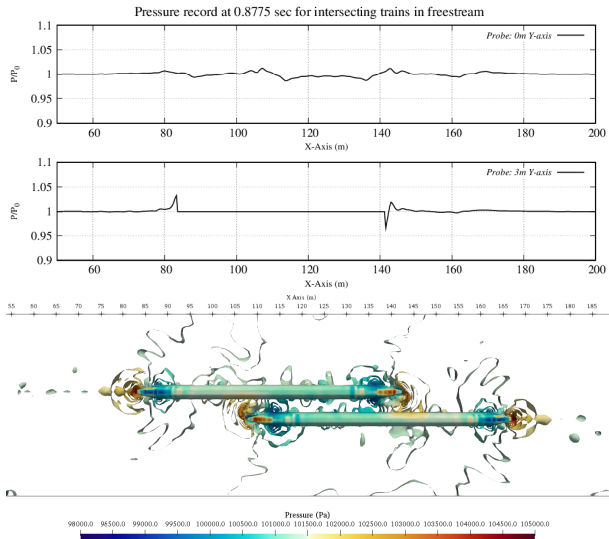
Pressure isosurfaces



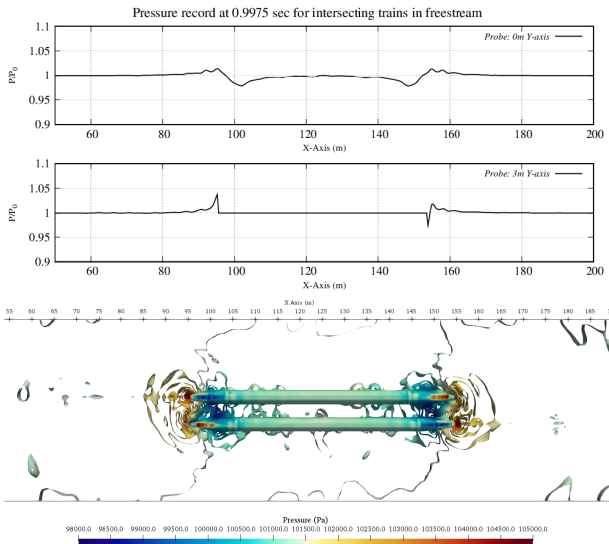
Pressure transects



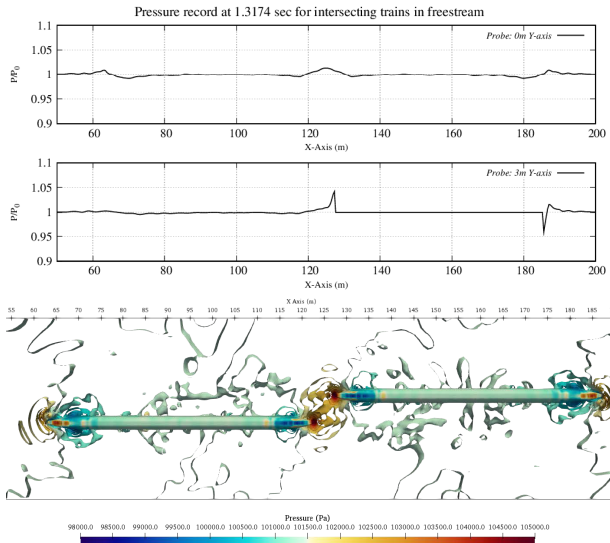
Pressure transects



Pressure transects

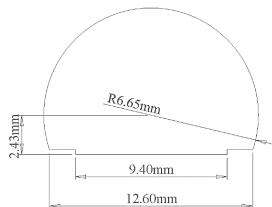


Pressure transects



Setup with realistic tunnel shape

- ▶ Two NGT2 trains again at velocities 100 m/s and -100 m/s
- ▶ Prototype straight double track tunnel of 640 m length, initial distance between centers of trains 820 m
- ▶ Base mesh of $1060 \times 36 \times 24$ for domain of $1060 \text{ m} \times 36 \text{ m} \times 24 \text{ m}$, three levels refined by $r_{1,2,3} = 2$
- ▶ On 96 cores Intel Xeon E5-2670 2.6 GHz a final $t_e = 5$ sec was reached after 84,651 sec wall time, i.e., 2257 h CPU

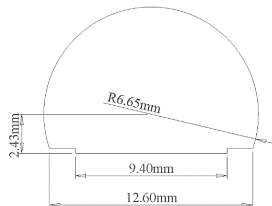


Tunnel shape



Setup with realistic tunnel shape

- ▶ Two NGT2 trains again at velocities 100 m/s and -100 m/s
- ▶ Prototype straight double track tunnel of 640 m length, initial distance between centers of trains 820 m
- ▶ Base mesh of $1060 \times 36 \times 24$ for domain of $1060 \text{ m} \times 36 \text{ m} \times 24 \text{ m}$, three levels refined by $r_{1,2,3} = 2$
- ▶ On 96 cores Intel Xeon E5-2670 2.6 GHz a final $t_e = 5 \text{ sec}$ was reached after 84,651 sec wall time, i.e., 2257 h CPU

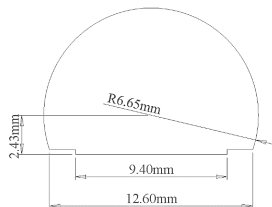


Tunnel shape

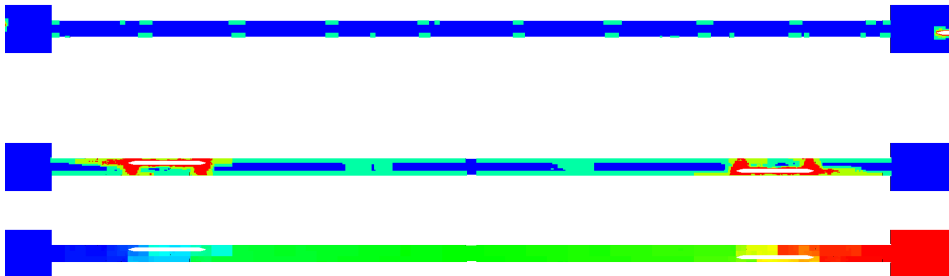


Setup with realistic tunnel shape

- ▶ Two NGT2 trains again at velocities 100 m/s and -100 m/s
- ▶ Prototype straight double track tunnel of 640 m length, initial distance between centers of trains 820 m
- ▶ Base mesh of $1060 \times 36 \times 24$ for domain of $1060 \text{ m} \times 36 \text{ m} \times 24 \text{ m}$, three levels refined by $r_{1,2,3} = 2$
- ▶ On 96 cores Intel Xeon E5-2670 2.6 GHz a final $t_e = 5$ sec was reached after 84,651 sec wall time, i.e., 2257 h CPU

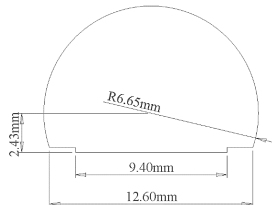


Tunnel shape

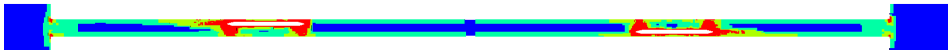


Setup with realistic tunnel shape

- ▶ Two NGT2 trains again at velocities 100 m/s and -100 m/s
- ▶ Prototype straight double track tunnel of 640 m length, initial distance between centers of trains 820 m
- ▶ Base mesh of $1060 \times 36 \times 24$ for domain of $1060 \text{ m} \times 36 \text{ m} \times 24 \text{ m}$, three levels refined by $r_{1,2,3} = 2$
- ▶ On 96 cores Intel Xeon E5-2670 2.6 GHz a final $t_e = 5$ sec was reached after 84,651 sec wall time, i.e., 2257 h CPU

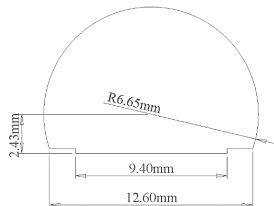


Tunnel shape



Setup with realistic tunnel shape

- ▶ Two NGT2 trains again at velocities 100 m/s and -100 m/s
- ▶ Prototype straight double track tunnel of 640 m length, initial distance between centers of trains 820 m
- ▶ Base mesh of $1060 \times 36 \times 24$ for domain of $1060 \text{ m} \times 36 \text{ m} \times 24 \text{ m}$, three levels refined by $r_{1,2,3} = 2$
- ▶ On 96 cores Intel Xeon E5-2670 2.6 GHz a final $t_e = 5 \text{ sec}$ was reached after 84,651 sec wall time, i.e., 2257 h CPU

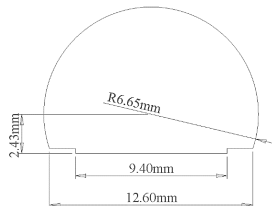


Tunnel shape

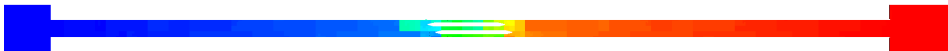
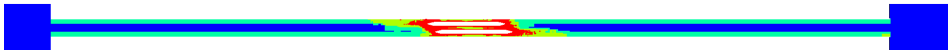


Setup with realistic tunnel shape

- ▶ Two NGT2 trains again at velocities 100 m/s and -100 m/s
- ▶ Prototype straight double track tunnel of 640 m length, initial distance between centers of trains 820 m
- ▶ Base mesh of $1060 \times 36 \times 24$ for domain of $1060 \text{ m} \times 36 \text{ m} \times 24 \text{ m}$, three levels refined by $r_{1,2,3} = 2$
- ▶ On 96 cores Intel Xeon E5-2670 2.6 GHz a final $t_e = 5 \text{ sec}$ was reached after 84,651 sec wall time, i.e., 2257 h CPU

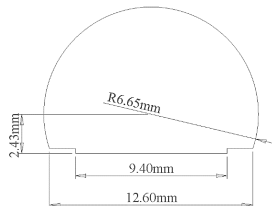


Tunnel shape

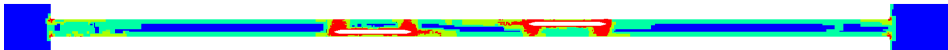


Setup with realistic tunnel shape

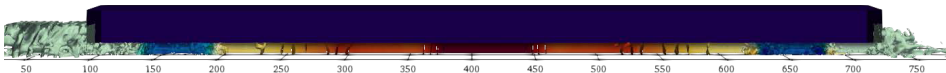
- ▶ Two NGT2 trains again at velocities 100 m/s and -100 m/s
- ▶ Prototype straight double track tunnel of 640 m length, initial distance between centers of trains 820 m
- ▶ Base mesh of $1060 \times 36 \times 24$ for domain of $1060 \text{ m} \times 36 \text{ m} \times 24 \text{ m}$, three levels refined by $r_{1,2,3} = 2$
- ▶ On 96 cores Intel Xeon E5-2670 2.6 GHz a final $t_e = 5$ sec was reached after 84,651 sec wall time, i.e., 2257 h CPU



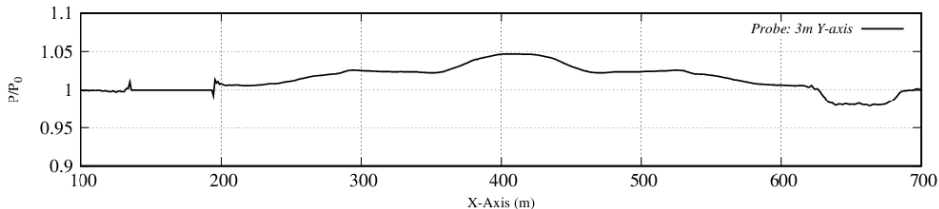
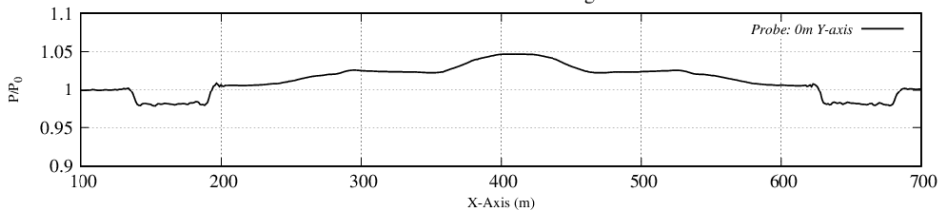
Tunnel shape



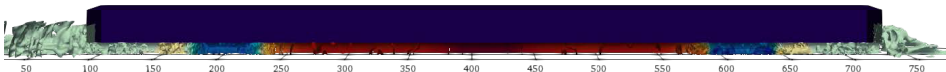
Pressure transects



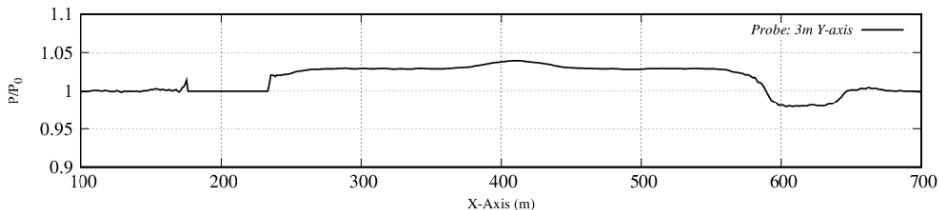
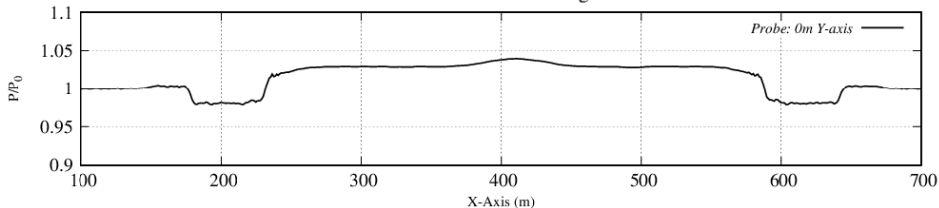
Pressure record at 1.39875 seconds for trains intersecting inside a double-track tunnel



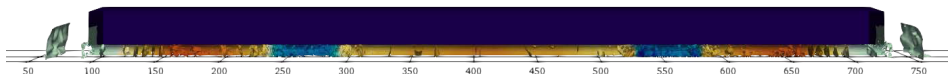
Pressure transects



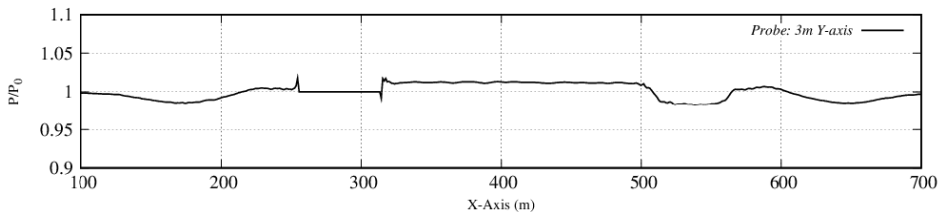
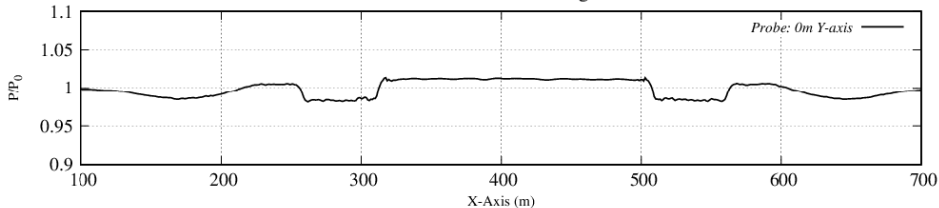
Pressure record at 1.7987 seconds for trains intersecting inside a double-track tunnel



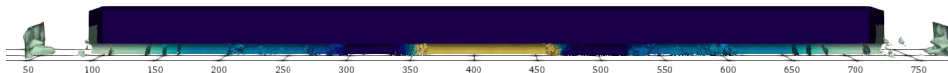
Pressure transects



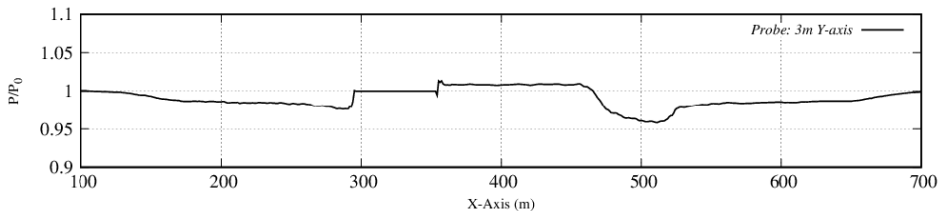
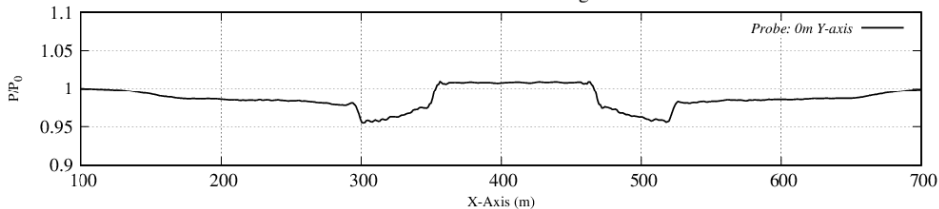
Pressure record at 2.5987 seconds for trains intersecting inside a double-track tunnel



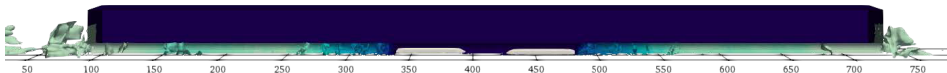
Pressure transects



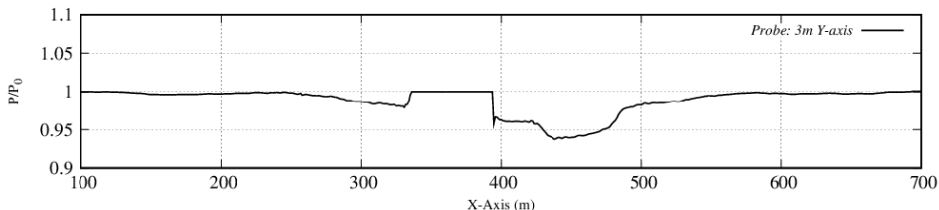
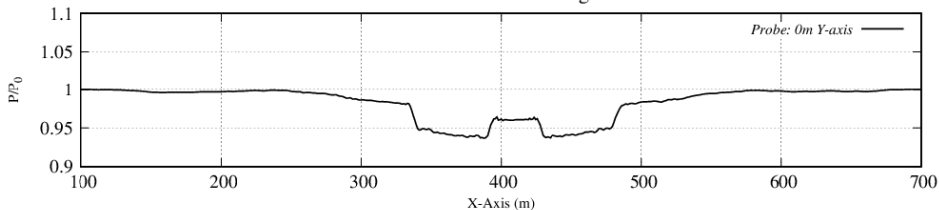
Pressure record at 2.9988 seconds for trains intersecting inside a double-track tunnel



Pressure transects



Pressure record at 3.3987 seconds for trains intersecting inside a double-track tunnel



Conclusions

- ▶ A Cartesian embedded boundary method for compressible flows with block-based adaptive mesh refinement is a highly efficient and scalable prediction tool for pressure and shock waves created in front of high-speed trains. This gives predictions of maximal loading.

Conclusions

- ▶ A Cartesian embedded boundary method for compressible flows with block-based adaptive mesh refinement is a highly efficient and scalable prediction tool for pressure and shock waves created in front of high-speed trains. This gives predictions of maximal loading.
- ▶ For predicting the flow around entire trains, the boundary layer growing over the train body needs to be considered.

Conclusions

- ▶ A Cartesian embedded boundary method for compressible flows with block-based adaptive mesh refinement is a highly efficient and scalable prediction tool for pressure and shock waves created in front of high-speed trains. This gives predictions of maximal loading.
- ▶ For predicting the flow around entire trains, the boundary layer growing over the train body needs to be considered.
- ▶ AMROC solvers for the compressible Navier-Stokes equations and even LES are already available, however, for this particular application a turbulent wall function on the embedded boundary first needs to be implemented. Such a wall function is currently work-in-progress for the LBM-LES solver.

References I

- [Barton et al., 2013] Barton, P. T., Deiterding, R., Meiron, D. I., and Pullin, D. I. (2013). Eulerian continuum model and adaptive finite-difference method for high-velocity impact and penetration problems. *J. Comput. Phys.*, 240:76–99.
- [Bell et al., 1994] Bell, J., Berger, M., Saltzman, J., and Welcome, M. (1994). Three-dimensional adaptive mesh refinement for hyperbolic conservation laws. *SIAM J. Sci. Comp.*, 15(1):127–138.
- [Berger, 1986] Berger, M. (1986). Data structures for adaptive grid generation. *SIAM J. Sci. Stat. Comput.*, 7(3):904–916.
- [Berger and Colella, 1988] Berger, M. and Colella, P. (1988). Local adaptive mesh refinement for shock hydrodynamics. *J. Comput. Phys.*, 82:64–84.
- [Berger and Rigoutsos, 1991] Berger, M. and Rigoutsos, I. (1991). An algorithm for point clustering and grid generation. *IEEE Transactions on Systems, Man, and Cybernetics*, 21(5):1278–1286.
- [Cai et al., 2018] Cai, X., Deiterding, R., Liang, J., Sun, M., and Mahmoudi, Y. (2018). Experimental and numerical investigations on propagating modes of detonations: detonation wave/boundary layer interaction. *Combust. Flame*, 190:201–215.
- [Cai et al., 2016] Cai, X., Liang, J., Deiterding, R., Che, Y., and Lin, Z. (2016). Adaptive mesh refinement based simulations of three-dimensional detonation combustion in supersonic combustible mixtures with a detailed reaction model. *Int. J. Hydrogen Energy*, 41:3222–3239.
- [Cerminara et al., 2018] Cerminara, A., Deiterding, R., and Sandham, N. (2018). Dns of hypersonic flow over porous surfaces with a hybrid method. In *AIAA Aerospace Sciences Meeting, AIAA Science and Technology Forum and Exposition*.
- [Cirak et al., 2007] Cirak, F., Deiterding, R., and Mauch, S. P. (2007). Large-scale fluid-structure interaction simulation of viscoplastic and fracturing thin shells subjected to shocks and detonations. *Computers & Structures*, 85(11-14):1049–1065.
- [Deiterding, 2003] Deiterding, R. (2003). *Parallel adaptive simulation of multi-dimensional detonation structures*. PhD thesis, Brandenburgische Technische Universität Cottbus.
- [Deiterding, 2005] Deiterding, R. (2005). Construction and application of an AMR algorithm for distributed memory computers. In Plewa, T., Linde, T., and Weirs, V. G., editors, *Adaptive Mesh Refinement - Theory and Applications*, volume 41 of *Lecture Notes in Computational Science and Engineering*, pages 361–372. Springer.
- [Deiterding, 2009] Deiterding, R. (2009). A parallel adaptive method for simulating shock-induced combustion with detailed chemical kinetics in complex domains. *Computers & Structures*, 87:769–783.

References II

- [Deiterding, 2011a] Deiterding, R. (2011a). Block-structured adaptive mesh refinement - theory, implementation and application. *European Series in Applied and Industrial Mathematics: Proceedings*, 34:97–150.
- [Deiterding, 2011b] Deiterding, R. (2011b). High-resolution numerical simulation and analysis of Mach reflection structures in detonation waves in low-pressure $\text{H}_2 : \text{O}_2 : \text{Ar}$ mixtures: a summary of results obtained with adaptive mesh refinement framework AMROC. *J. Combustion*, 2011:738969.
- [Deiterding and Bader, 2005] Deiterding, R. and Bader, G. (2005). High-resolution simulation of detonations with detailed chemistry. In Warnecke, G., editor, *Analysis and Numerics for Conservation Laws*, pages 69–91. Springer.
- [Deiterding et al., 2009a] Deiterding, R., Cirak, F., and Mauch, S. P. (2009a). Efficient fluid-structure interaction simulation of viscoplastic and fracturing thin-shells subjected to underwater shock loading. In Hartmann, S., Meister, A., Schäfer, M., and Turek, S., editors, *Int. Workshop on Fluid-Structure Interaction. Theory, Numerics and Applications, Herrsching am Ammersee 2008*, pages 65–80. kassel university press GmbH.
- [Deiterding et al., 2007] Deiterding, R., Cirak, F., Mauch, S. P., and Meiron, D. I. (2007). A virtual test facility for simulating detonation- and shock-induced deformation and fracture of thin flexible shells. *Int. J. Multiscale Computational Engineering*, 5(1):47–63.
- [Deiterding et al., 2009b] Deiterding, R., Domingues, M. O., Gomes, S. M., Roussel, O., and Schneider, K. (2009b). Adaptive multiresolution or adaptive mesh refinement? A case study for 2D Euler equations. *European Series in Applied and Industrial Mathematics: Proceedings*, 29:28–42.
- [Deiterding et al., 2006] Deiterding, R., Radovitzky, R., Mauch, S. P., Noels, L., Cummings, J. C., and Meiron, D. I. (2006). A virtual test facility for the efficient simulation of solid materials under high energy shock-wave loading. *Engineering with Computers*, 22(3-4):325–347.
- [Deiterding and Wood, 2016] Deiterding, R. and Wood, S. L. (2016). Predictive wind turbine simulation with an adaptive lattice Boltzmann method for moving boundaries. *J. Phys. Conf. Series*, 753:082005.
- [Feldhusen et al., 2016] Feldhusen, K., Deiterding, R., and Wagner, C. (2016). A dynamically adaptive lattice Boltzmann method for thermal convection problems. *J. Applied Math. and Computer Science*, 26:735–747.
- [Fragner and Deiterding, 2016] Fragner, M. M. and Deiterding, R. (2016). Investigating cross-wind stability of high speed trains with large-scale parallel cfd. *Int. J. Comput. Fluid Dynamics*, 30:402–407.

References III

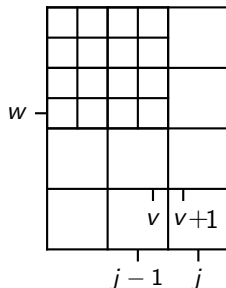
- [Fragner and Deiterding, 2017] Fragner, M. M. and Deiterding, R. (2017). Investigating side-wind stability of high speed trains using high resolution large eddy simulations and hybrid models. In Diez, P., Neittaanmäki, P., Periaux, J., Tuovinen, T., and Bräysy, O., editors, *Computational Methods in Applied Sciences*, volume 45, pages 223–241. Springer.
- [Gomes et al., 2015] Gomes, A. K. F., Domingues, M. O., Schneider, K., Mendes, O., and Deiterding, R. (2015). An adaptive multiresolution method for ideal magnetohydrodynamics using divergence cleaning with parabolic-hyperbolic correction. *Applied Numerical Mathematics*, 95:199–213.
- [Lombardini and Deiterding, 2010] Lombardini, M. and Deiterding, R. (2010). Large-eddy simulation of Richtmyer-Meshkov instability in a converging geometry. *Physics of Fluids*, 22(9):091112.
- [Mauch, 2003] Mauch, S. P. (2003). *Efficient Algorithms for Solving Static Hamilton-Jacobi Equations*. PhD thesis, California Institute of Technology.
- [Pantano et al., 2007] Pantano, C., Deiterding, R., Hill, D. J., and Pullin, D. I. (2007). A low-numerical dissipation patch-based adaptive mesh refinement method for large-eddy simulation of compressible flows. *J. Comput. Phys.*, 221(1):63–87.
- [Perotti et al., 2013] Perotti, L. E., Deiterding, R., Inaba, K., Shepherd, J. E., and Ortiz, M. (2013). Elastic response of water-filled fiber composite tubes under shock wave loading. *Int. J. Solids and Structures*, 50(3-4):473–486.
- [Sethian, 1999] Sethian, J. A. (1999). *Level set methods and fast marching methods*. Cambridge University Press, Cambridge, New York.
- [Souza Lopes et al., 2018] Souza Lopes, M. M., Deiterding, R., Gomes, A. K. F., Mendes, O., and Domingues, M. O. (2018). An ideal compressible magnetohydrodynamic solver with parallel block-structured adaptive mesh refinement. *Computers & Fluids*. in press.
- [Wan et al., 2017] Wan, Q., Jeon, H., Deiterding, R., and Eliasson, V. (2017). Numerical and experimental investigation of oblique shock wave reflection off a water wedge. *J. Fluid Mech.*, 826:732–758.
- [Ziegler et al., 2011] Ziegler, J. L., Deiterding, R., Shepherd, J. E., and Pullin, D. I. (2011). An adaptive high-order hybrid scheme for compressive, viscous flows with detailed chemistry. *J. Comput. Phys.*, 230(20):7598–7630.
- [Zonglin et al., 2002] Zonglin, J., Matsuoka, K., Sasoh, A., and Takayama, K. (2002). Numerical and experimental investigation of wave dynamics processes in high-speed train/tunnels. *Chinese Journal of Mechanics Press*, 18(3):210–226.

Conservative flux correction

Example: Cell j, k

$$\begin{aligned} \check{\mathbf{Q}}_{jk}^l(t + \Delta t_l) = & \mathbf{Q}_{jk}^l(t) - \frac{\Delta t_l}{\Delta x_{1,l}} \left(\mathbf{F}_{j+\frac{1}{2},k}^l - \frac{1}{r_{l+1}^2} \sum_{\kappa=0}^{r_{l+1}-1} \sum_{\iota=0}^{r_{l+1}-1} \mathbf{F}_{v+\frac{1}{2},w+\iota}^{l+1}(t + \kappa \Delta t_{l+1}) \right) \\ & - \frac{\Delta t_l}{\Delta x_{2,l}} \left(\mathbf{G}_{j,k+\frac{1}{2}}^l - \mathbf{G}_{j,k-\frac{1}{2}}^l \right) \end{aligned}$$

Correction pass:



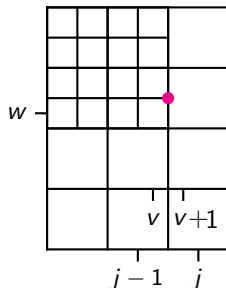
Conservative flux correction

Example: Cell j, k

$$\begin{aligned} \check{\mathbf{Q}}_{jk}^l(t + \Delta t_l) = & \mathbf{Q}_{jk}^l(t) - \frac{\Delta t_l}{\Delta x_{1,l}} \left(\mathbf{F}_{j+\frac{1}{2},k}^l - \frac{1}{r_{l+1}^2} \sum_{\kappa=0}^{r_{l+1}-1} \sum_{\iota=0}^{r_{l+1}-1} \mathbf{F}_{v+\frac{1}{2},w+\iota}^{l+1}(t + \kappa \Delta t_{l+1}) \right) \\ & - \frac{\Delta t_l}{\Delta x_{2,l}} \left(\mathbf{G}_{j,k+\frac{1}{2}}^l - \mathbf{G}_{j,k-\frac{1}{2}}^l \right) \end{aligned}$$

Correction pass:

$$1. \delta \mathbf{F}_{j-\frac{1}{2},k}^{l+1} := -\mathbf{F}_{j-\frac{1}{2},k}^l$$



Conservative flux correction

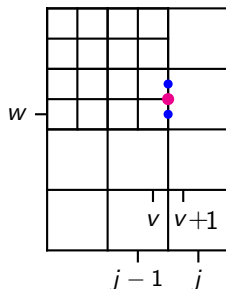
Example: Cell j, k

$$\begin{aligned} \check{\mathbf{Q}}_{jk}^l(t + \Delta t_l) = & \mathbf{Q}_{jk}^l(t) - \frac{\Delta t_l}{\Delta x_{1,l}} \left(\mathbf{F}_{j+\frac{1}{2},k}^l - \frac{1}{r_{l+1}^2} \sum_{\kappa=0}^{r_{l+1}-1} \sum_{\iota=0}^{r_{l+1}-1} \mathbf{F}_{v+\frac{1}{2},w+\iota}^{l+1}(t + \kappa \Delta t_{l+1}) \right) \\ & - \frac{\Delta t_l}{\Delta x_{2,l}} \left(\mathbf{G}_{j,k+\frac{1}{2}}^l - \mathbf{G}_{j,k-\frac{1}{2}}^l \right) \end{aligned}$$

Correction pass:

$$1. \delta \mathbf{F}_{j-\frac{1}{2},k}^{l+1} := -\mathbf{F}_{j-\frac{1}{2},k}^l$$

$$2. \delta \mathbf{F}_{j-\frac{1}{2},k}^{l+1} := \delta \mathbf{F}_{j-\frac{1}{2},k}^{l+1} + \frac{1}{r_{l+1}^2} \sum_{\iota=0}^{r_{l+1}-1} \mathbf{F}_{v+\frac{1}{2},w+\iota}^{l+1}(t + \kappa \Delta t_{l+1})$$



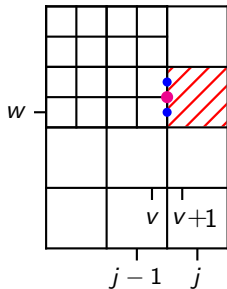
Conservative flux correction

Example: Cell j, k

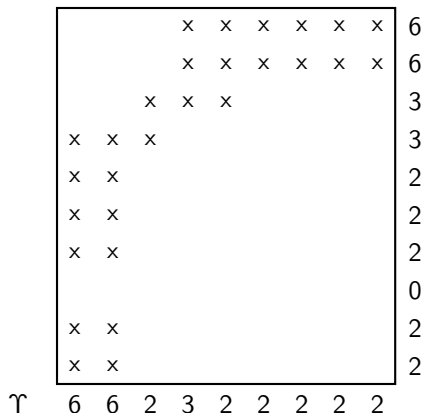
$$\begin{aligned} \check{\mathbf{Q}}_{jk}^l(t + \Delta t_l) = & \mathbf{Q}_{jk}^l(t) - \frac{\Delta t_l}{\Delta x_{1,l}} \left(\mathbf{F}_{j+\frac{1}{2},k}^l - \frac{1}{r_{l+1}^2} \sum_{\kappa=0}^{r_{l+1}-1} \sum_{\iota=0}^{r_{l+1}-1} \mathbf{F}_{v+\frac{1}{2},w+\iota}^{l+1}(t + \kappa \Delta t_{l+1}) \right) \\ & - \frac{\Delta t_l}{\Delta x_{2,l}} \left(\mathbf{G}_{j,k+\frac{1}{2}}^l - \mathbf{G}_{j,k-\frac{1}{2}}^l \right) \end{aligned}$$

Correction pass:

1. $\delta \mathbf{F}_{j-\frac{1}{2},k}^{l+1} := -\mathbf{F}_{j-\frac{1}{2},k}^l$
2. $\delta \mathbf{F}_{j-\frac{1}{2},k}^{l+1} := \delta \mathbf{F}_{j-\frac{1}{2},k}^{l+1} + \frac{1}{r_{l+1}^2} \sum_{\iota=0}^{r_{l+1}-1} \mathbf{F}_{v+\frac{1}{2},w+\iota}^{l+1}(t + \kappa \Delta t_{l+1})$
3. $\check{\mathbf{Q}}_{jk}^l(t + \Delta t_l) := \mathbf{Q}_{jk}^l(t + \Delta t_l) + \frac{\Delta t_l}{\Delta x_{1,l}} \delta \mathbf{F}_{j-\frac{1}{2},k}^{l+1}$



Clustering by signatures



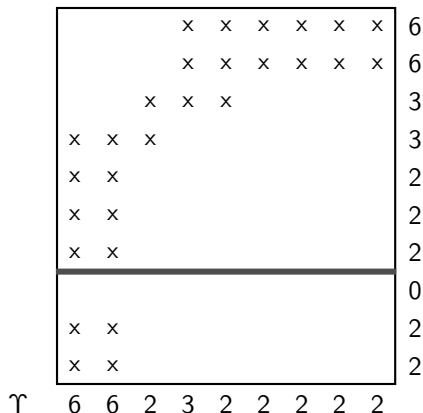
Υ Flagged cells per row/column

Δ Second derivative of Υ , $\Delta = \Upsilon_{\nu+1} - 2\Upsilon_{\nu} + \Upsilon_{\nu-1}$

Technique from image detection: [Bell et al., 1994], see also

[Berger and Rigoutsos, 1991], [Berger, 1986]

Clustering by signatures



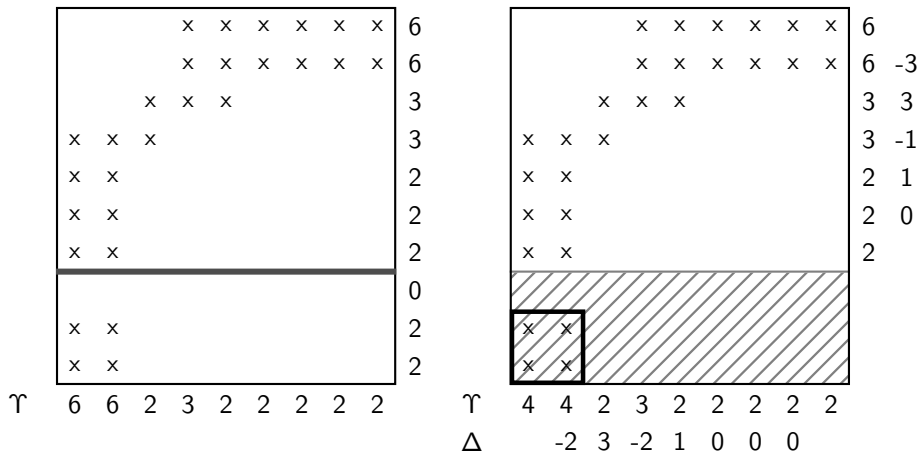
Υ Flagged cells per row/column

Δ Second derivative of Υ , $\Delta = \Upsilon_{\nu+1} - 2\Upsilon_{\nu} + \Upsilon_{\nu-1}$

Technique from image detection: [Bell et al., 1994], see also

[Berger and Rigoutsos, 1991], [Berger, 1986]

Clustering by signatures



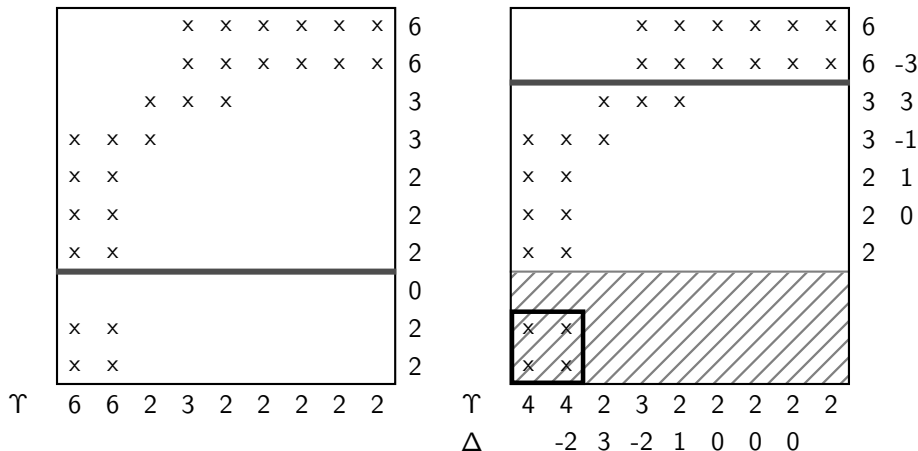
Υ Flagged cells per row/column

Δ Second derivative of Υ , $\Delta = \Upsilon_{\nu+1} - 2\Upsilon_{\nu} + \Upsilon_{\nu-1}$

Technique from image detection: [Bell et al., 1994], see also

[Berger and Rigoutsos, 1991], [Berger, 1986]

Clustering by signatures

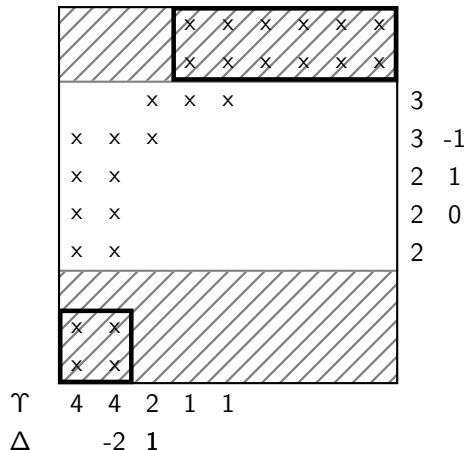


Υ Flagged cells per row/column

Δ Second derivative of Υ , $\Delta = \Upsilon_{\nu+1} - 2\Upsilon_{\nu} + \Upsilon_{\nu-1}$

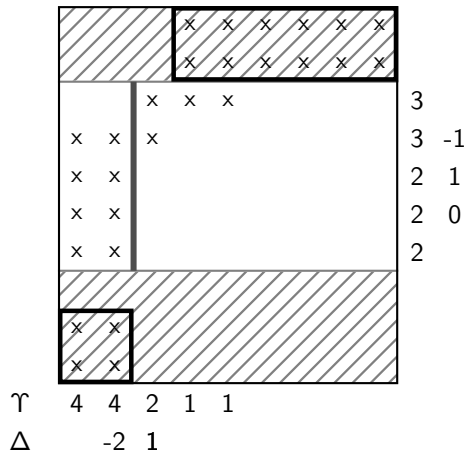
Technique from image detection: [Bell et al., 1994], see also

[Berger and Rigoutsos, 1991], [Berger, 1986]



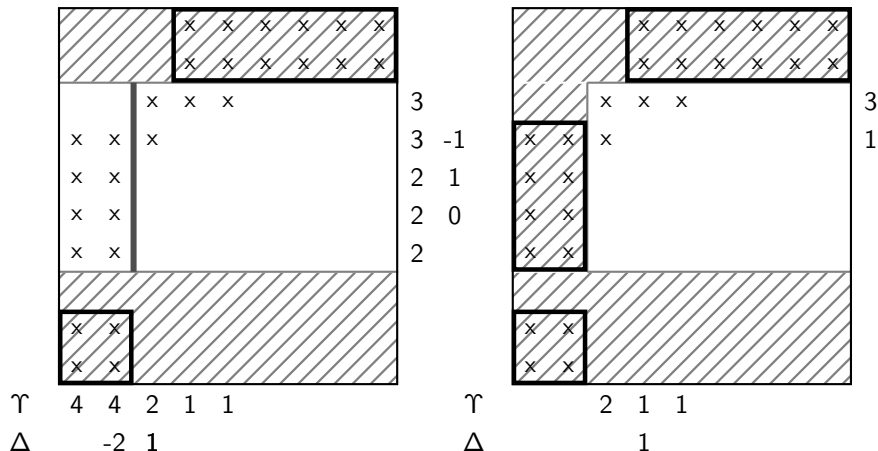
Recursive generation of $\check{G}_{l,m}$

1. 0 in Υ
2. Largest difference in Δ
3. Stop if ratio between flagged and unflagged cell $> \eta_{tol}$



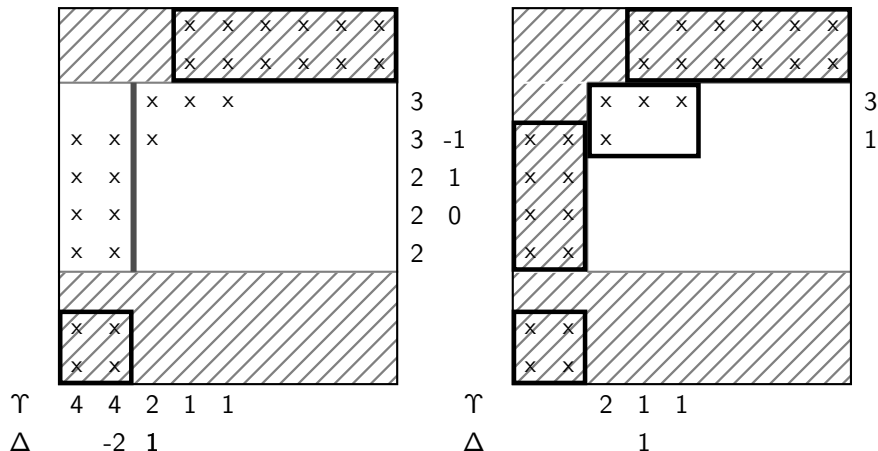
Recursive generation of $\check{G}_{l,m}$

1. 0 in Υ
2. Largest difference in Δ
3. Stop if ratio between flagged and unflagged cell $> \eta_{tol}$



Recursive generation of $\check{G}_{l,m}$

1. 0 in Υ
2. Largest difference in Δ
3. Stop if ratio between flagged and unflagged cell $> \eta_{tol}$



Recursive generation of $\check{G}_{l,m}$

1. 0 in Υ
2. Largest difference in Δ
3. Stop if ratio between flagged and unflagged cell $> \eta_{tol}$

Closest point transform algorithm

The signed distance φ to a surface \mathcal{I} satisfies the eikonal equation [Sethian, 1999]

$$|\nabla\varphi| = 1 \quad \text{with} \quad \varphi|_{\mathcal{I}} = 0$$

Solution smooth but non-differentiable across characteristics.

Closest point transform algorithm

The signed distance φ to a surface \mathcal{I} satisfies the eikonal equation [Sethian, 1999]

$$|\nabla\varphi| = 1 \quad \text{with} \quad \varphi|_{\mathcal{I}} = 0$$

Solution smooth but non-differentiable across characteristics.

Distance computation trivial for non-overlapping elementary shapes but difficult to do efficiently for triangulated surface meshes:

- ▶ Geometric solution approach with closest-point-transform algorithm [Mauch, 2003]

Closest point transform algorithm

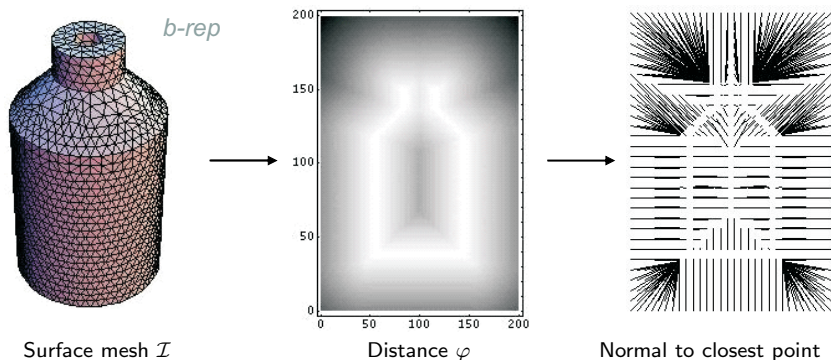
The signed distance φ to a surface \mathcal{I} satisfies the eikonal equation [Sethian, 1999]

$$|\nabla \varphi| = 1 \quad \text{with} \quad \varphi|_{\mathcal{I}} = 0$$

Solution smooth but non-differentiable across characteristics.

Distance computation trivial for non-overlapping elementary shapes but difficult to do efficiently for triangulated surface meshes:

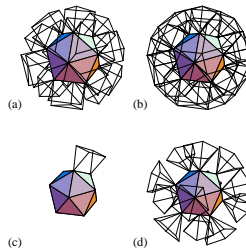
- Geometric solution approach with closest-point-transform algorithm [Mauch, 2003]



The characteristic / scan conversion algorithm

1. Build the characteristic polyhedrons for the surface mesh

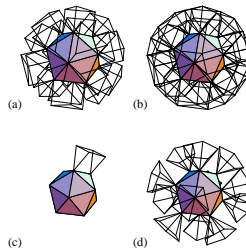
Characteristic polyhedra for faces, edges, and vertices



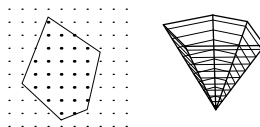
The characteristic / scan conversion algorithm

1. Build the characteristic polyhedrons for the surface mesh
2. For each face/edge/vertex
 - 2.1 Scan convert the polyhedron.

Characteristic polyhedra for faces, edges, and vertices



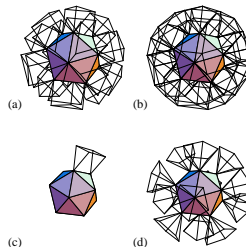
Slicing and scan conversion of apolygon



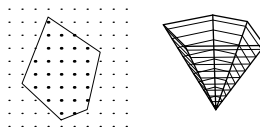
The characteristic / scan conversion algorithm

1. Build the characteristic polyhedrons for the surface mesh
2. For each face/edge/vertex
 - 2.1 Scan convert the polyhedron.
 - 2.2 Compute distance to that primitive for the scan converted points

Characteristic polyhedra for faces, edges, and vertices



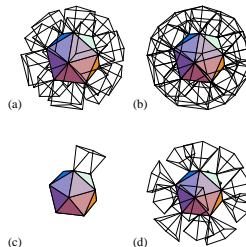
Slicing and scan conversion of apolygon



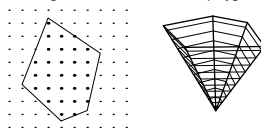
The characteristic / scan conversion algorithm

1. Build the characteristic polyhedrons for the surface mesh
2. For each face/edge/vertex
 - 2.1 Scan convert the polyhedron.
 - 2.2 Compute distance to that primitive for the scan converted points
3. Computational complexity.
 - ▶ $O(m)$ to build the b-rep and the polyhedra.
 - ▶ $O(n)$ to scan convert the polyhedra and compute the distance, etc.

Characteristic polyhedra for faces, edges, and vertices



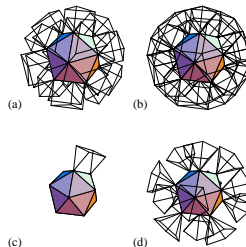
Slicing and scan conversion of apolygon



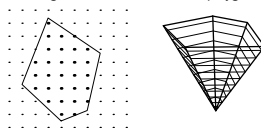
The characteristic / scan conversion algorithm

1. Build the characteristic polyhedrons for the surface mesh
2. For each face/edge/vertex
 - 2.1 Scan convert the polyhedron.
 - 2.2 Compute distance to that primitive for the scan converted points
3. Computational complexity.
 - ▶ $O(m)$ to build the b-rep and the polyhedra.
 - ▶ $O(n)$ to scan convert the polyhedra and compute the distance, etc.
4. Problem reduction by evaluation only within specified max. distance

Characteristic polyhedra for faces, edges, and vertices



Slicing and scan conversion of apolygon



[Mauch, 2003], see also
[Deiterding et al., 2006]